Liquid spray injection in the expansion volume of a CO$_2$ high voltage circuit breaker

Paolo ERRANTE[*,1,2], Christophe CORRE[1,2], Samir MAKHLOUF[2]
[1]LMFA, Ecole Centrale de Lyon, France
[2]SuperGrid Institute, Villeurbanne, France
*Corresponding author: Paolo.Errante@supergrid-institute.com

Abstract

Most high voltage gas circuit breakers (HVCB) in operation use SF$_6$ as the arc interruption medium because of its high dielectric strength and good arc interruption properties. However, SF$_6$ also displays a high global warming potential which motivates the investigation of possible alternatives to this gas. The performance of CO$_2$ as an interruption medium in HVCB has been previously examined in the literature and it was established the CO$_2$ intrinsic performance was clearly worse than that of SF6. Optimization of circuit breaker design to account for the specific properties of CO$_2$ is likely to bring some improvement, although without matching the performance and small size of designs optimized for SF$_6$. To further improve the interruption properties of a CO$_2$ circuit breaker, a spray of a selected liquid, typically a mineral oil, is injected in the circuit breaker expansion volume so as to: i) favor the pressure increase mechanism leading to a more efficient arc expansion process; ii) generate a mixture likely to ensure a better heat release at current-zero and improve the dielectric performance. A spray injection device has been experimentally developed and is complemented with a numerical simulation of the interaction between the spray and the hot gas flow within the expansion volume. The numerical model relies on an Eulerian-Lagrangian description of the flow which combines a RANS modeling of the gaseous phase and a Lagrangian description of the discrete phase, including a turbulent dispersion model and an evaporation model of Abramzon-Sirignano type for the spray droplets. Both descriptions are coupled through a two-way approach which accounts for the effects of the continuous phase on the droplets and the retro-action of the droplets on the carrier phase. The computational domain includes the expansion volume and part of the nozzle connecting the arc region to the expansion volume with inlet / outlet conditions applied on the nozzle boundary obtained from a full computation of the HVCB, including the plasma region, performed with a dedicated software. The thermodynamic description of the mixture between CO$_2$, Polytetrafluoroethylene (PTFE) vapour resulting from the ablation of the PTFE nozzle walls and oil vapour from the evaporating spray droplets relies on look-up tables. Numerical simulations are performed and analyzed for various spray injection conditions in order to identify an optimal mixture configuration.

Keywords
high voltage circuit breaker, expansion volume, gas mixture, spray injection

Introduction

The protection of electric distribution and transmission networks nowadays widely relies on high-voltage circuit breakers. Whenever AC current transfers must be interrupted, an electrical arc is generated due to separation of two contacts. The arc's energy release provokes the ablation of the polytetrafluoroethylene (PTFE) components. These vapours are mixed together with a surrounding gas and channeled through an expansion volume where the hot stream mixes with a fresh gas. Approaching the next current-zero, the pressure gradient between the volume and the arcing zone is reversed. The cooled gas is then blown on the arc zone to decrease the temperature of plasma. Once the arc is quenched, a potential difference, known as transient recovery voltage (TRV), appears in between the arcing contacts. At this point, the dielectric recovery of the medium would avoid a re-ignition of the electric arc due to the TRV. The dielectric breakdown of the medium depends on electrical charges release events, which are less likely to occur when the gas mixture temperature is lower and its electronegativity is higher. For these reasons, an improved HVCB performance could rely on a mixing process inside the expansion volume, which should deliver not only the flux of a colder gas but also a quantity of chemical species as well. In the present study, the injection of a liquid spray inside the expansion volume is investigated to produce these beneficial effects.

Physical and numerical description of the flow inside the HVCB expansion volume

An overview of the axisymmetric computational flow domain is provided in Figure 1. The domain is restricted to the expansion volume of the HVCB and the associated channel so as to avoid the need to describe in detail the complex arcing region. The arc is modeled through a transient pressure boundary condition at the connection between the channel and the arcing zone, which is obtained from a numerical simulation of the whole HVCB, including the arcing region, but performed for a coarser description of the expansion volume. In the present study, the computational grid displayed in Figure 1 is made of a mix of rectangular (near-wall) cells near the solid walls (boundary-layer type mesh) and triangular cells in the inner volume for a total of 32850 cells. The gas initially entering the flow domain is a mixture of the following components:

- CO_2, which fills the device before arc ignition,

- C_2F_4 (tetrafluoroethylene or TFE), which is generated from PTFE ablation during the arcing time.

At later times, the gas mixture also includes the vapour produced by the vaporization of oil droplets inside the expansion volume (see next section). The compressible unsteady Reynolds Averaged Navier-Stokes equations (URANS system) are solved to describe the evolution of the gas mixture flow field. The mass, momentum and energy equations of the mixture are completed with transport equations for the turbulent quantities k and ε, the standard k-ε turbulence model being used to close the URANS system. The mixture composition evolution is computed by solving two additional transport equations for the mass fraction y_i of two of the components, the third one being directly derived from $\sum_{i=1}^{3} y_i = 1$.
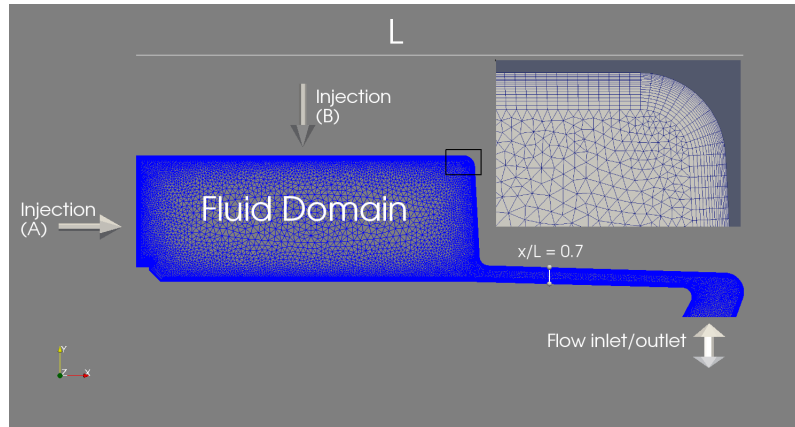
**Figure 1.** Schematic view of the computational domain, boundary conditions and post-processing sections.

The thermodynamic properties and transport coefficients of the mixture between CO_2, C_2F_4 and oil have been computed using an advanced Equation of State for mixture pressure and temperature, varying respectively between 4 and 64 bar by step of 4 bar and between $300\,K$ and $30000\,K$ by step of $10\,K$, and the combination of mass fraction displayed in Figure 2. The corresponding values have been stored in Look-up Tables (LuT) which are then called by the CFD solver in order to compute properties at any point of the thermodynamic space. In the context of HVCB simulations, several CFD studies rely on the LuT approach [1] [2], [3] [4] [5]. However, these works do not provide details on the interpolation process applied to derive thermodynamic properties. As pointed out by few authors in the literature [6] [7] [8], care must be taken to use an interpolation method which respects thermodynamic consistency and stability criteria in order to be physically meaningful and to prevent the occurrence of spurious thermodynamic states. In the present work, the available thermodynamic potential from which all useful thermodynamic quantities can be consistently derived is Gibbs free energy, $g(p,T)$ in the case of a pure substance. An interpolation $\widetilde{g}(p,T)$ is built from the tabulated values of g and its successive first and second partial derivatives with respect to p and T (derived from tabulated thermodynamic quantities such as specific volume v, entropy s, heat capacities c_p, c_v and speed of sound a) using a bi-quintic Hermite interpolation inspired from [8]. Once the polynomial representation of $\widetilde{g}(p,T)$ is available, the successive derivatives of $\widetilde{g}(p,T)$ with respect to p and T are readily computed and can be used to compute all thermodynamic quantities of interest in a consistent and stable way. The approach is extended to the case of the gas mixture under study by combining the polynomial interpolation on p and T with a simple interpolation on the mass fractions y_i. Relevant User-Defined Functions are developed to couple this thermodynamic
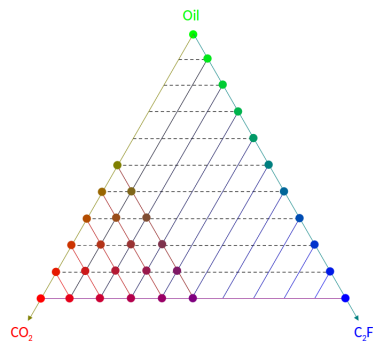
Figure 2. Overview of the various compositions of the CO_2, C_2F_4 and oil mixture for which a LuT is available for the thermodynamic quantities and transport properties. The vertices of the large triangle correspond to pure fluids.

description with the Ansys Fluent commercial CFD solver used to perform the present numerical simulations.

The second-order upwind Roe scheme with limited MUSCL extrapolation is applied to the solution of the governing equations. For the sake of robustness, a first-order Euler implicit time-marching scheme is applied with a time step size $\Delta t = 1 \mu s$. Note the partial derivatives of enthalpy needed to compute the Jacobian matrix appearing in the implicit stage are also derived from the polynomial representation $\widetilde{g}(p, T)$. The calculation is performed over a total time $t = 16\,ms$, during which the flow properties at the inlet / outlet boundary of the channel connecting the expansion volume to the arcing zone are imposed from another calculation performed on the full HVCB (but with a much coarser description of the expansion volume with respect to the one used in the present detailed analysis of the flow dynamics in the expansion volume). Such an approach has also been successfully applied by [1] when studying a similar configuration (with SF_6 as working fluid). The initial fluid (pure CO_2) inside the expansion volume is considered stagnant at atmospheric pressure and $300\,K$. The typical temperature of the gas (essentially C_2F_4) flowing inside the domain is about $3500\,K$. The ability of this simplified modeling to predict with reasonable accuracy the pressure dynamics inside the expansion volume of the HVCB is illustrated in Fig.3.
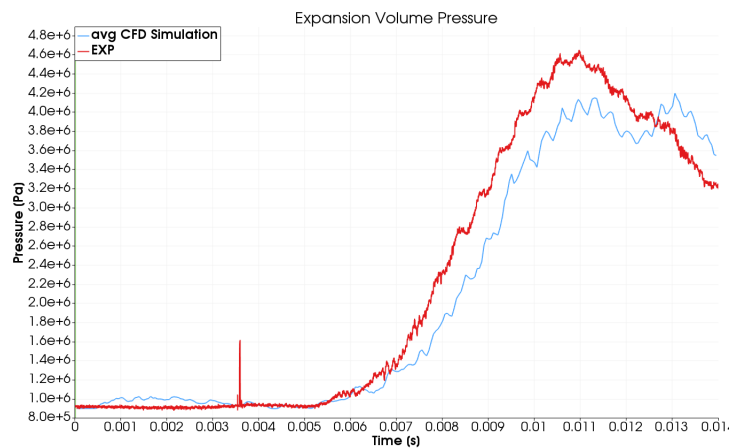
Figure 3. Experimental and simulated pressure evolution inside the expansion volume for the baseline configuration (without spray injection).

Spray injection

In order to enhance the arc interrupting properties of CO_2 a liquid spray of mineral oil is injected in the expansion volume. The liquid spray evolution is described in a Lagrangian framework well adapted to the modelling of this dispersed phase. Oil droplets are represented as point-like bodies, namely parcels, which move across the gaseous domain in a Lagrangian frame. The droplet behaviour or trajectory is described by a set of Ordinary Differential Equations (ODEs), describing mass, force and thermal balances. Liquid-gas interactions are defined using a two-way coupling approach, where the gas flow induces aerodynamics forces on droplets while, reversely, droplets travelling along their trajectories exchange mass and energy with the gaseous phase. This retroaction is described by source terms included in the URANS equations governing the carrier phase. In the case of a turbulent gas flow, a turbulent dispersion model (Discrete Random Walk) is introduced to take into account the effect of the gas fluctuating velocities on droplet motion. Moreover liquid-gas heat transfers are described by convective and evaporative models, which express the transport phenomena occurring at the droplet-gas interface. A number of experimental setups have been developed and exploited to perform reference measurements (*e.g.* [9]) which made it possible to calibrate and validate Eulerian-Lagrangian solvers so as to achieve quite accurate prediction of droplets kinematics and granulometry (see for instance [10] [11]).

Parcels are numerically released by point-like sources positioned along the spray nozzle exit surface (see next section for the location of the spray inside the expansion volume). From each of these points, velocity, temperature, diameter and mass flow rate of parcels can be assigned. Droplet size-velocity measurements are currently being performed for an injection system developed in the framework of an experimental study on spray injection inside the expansion volume of a HVCB. The preliminary calculations performed in the next section make use of a population of droplets defined accordingly to the experimental (SP2) measurements collected by Masri and Gounder [9]; the droplets characteristics are fixed in time and vary from one release point to the other. The liquid mass-flow rate is imposed equal to $5.65 \cdot 10^{-4}\,kgs^{-1}$. Oil droplets are released during the whole physical time of calculation $(t = 16\,ms)$.

Preliminary analysis of two spray injection configurations

Several parameters can be identified which influence the temperature and mixture composition during the interaction between the hot gas initially blown into the expansion volume and the liquid spray : size-velocity distribution

of the injected droplets, physical properties of the liquid, liquid mass-flow rate, injection starting time and duration, spray location. In the present analysis, three configurations are studied. In the first configuration, no spray injection is applied - the fluid is a CO_2 - C_2F_4 mixture. This reference configuration provides a baseline scenario for the development of the main flow-field features. The other two configurations include spray injection and differ only by the location of the spray injection. As described in Figure 1, configuration A corresponds to a spray injected on the wall of the expansion volume opposite to the channel connecting the volume with the arcing region, while configuration B corresponds to a spray injection located on the upper (or outer) wall at mid-distance between the channel exit and the opposite wall. Furthermore we want to observe how the introduction of a spray injection could affect the flow field. We propose then two additional configurations, named A and B, in which we release parcels from two different locations as depicted in Fig.1. In both cases, the evaporation of droplets will create oil vapour which will be then described as a third species in the gas mixture; the corresponding consistent interpolation process between LuT is then applied to compute the mixture thermodynamic properties and transport coefficients.

Figure 4 displays the time evolution of the normal velocity at the inlet/outlet boundary. It can be observed the fluid is first pushed inside the domain, during the 2 first milliseconds . Around $t = 2\,ms$ the flow direction starts to reverse and the outflow initiates. Around $t = 7\,ms$ and $13\,ms$ other flow reversal events take place but, unlike the initial in-flow, they are not sufficient to sustain the hot-gas flow up to the expansion volume.
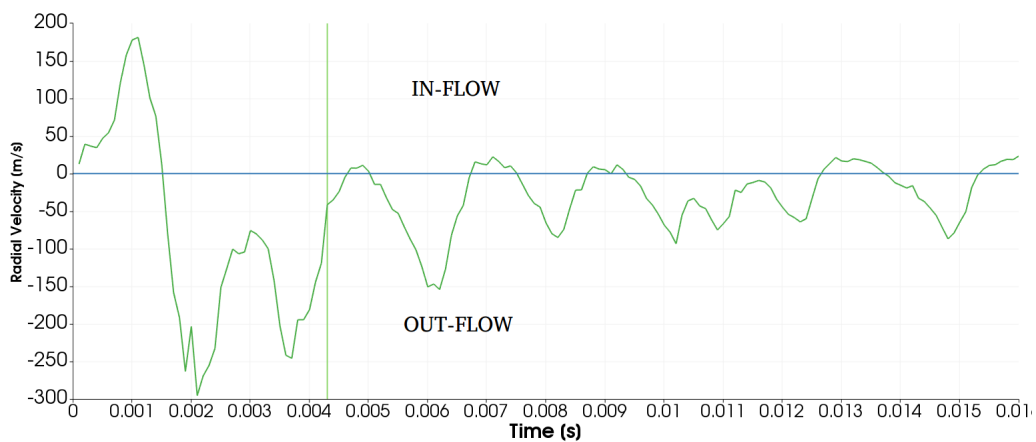
Figure 4. Evolution of the mean normal velocity at the inlet/outlet boundary as a function of the physical time.

Figure 5 displays the temperature field during the initial compression and expansion phases : the hot fluid (C_2F_4) first invades the expansion volume and mixes with the fresh gas (pure CO_2 for the no-injection case, mixture of CO_2 and oil vapour for injection cases A and B). Once the pressure in the volume becomes larger than the inlet pressure, the fluid flow reverses and the expansion phase starts : some fresh fluid is aspired through the channel while a vortical structure transporting TFE detaches from the channel to move inside the core of the expansion volume. A comparison between the reference no-injection solution and the flow fields computed for injection A and injection B indicates a very limited influence of the injected droplets on the temperature distribution inside the expansion volume - which is consistent with the small liquid mass injected.

Let us now use the no-injection axial (x component) velocity field to keep track of the fluid motion (the impact of the droplets on the gas mixture dynamics for configurations A and B remaining limited despite the two-way coupling process applied) while analyzing the spray injection features for configurations A and B at successive times $t = 1.2\,ms$, $2.4\,ms$ and $6.4\,ms$ in Figure 6. During the in-flow phase (negative value of axial velocity at the channel mouth inside the expansion volume, see top picture in Fig.6), droplets in configuration B are transported by the carrier phase towards the back-side of the domain while in configuration A the liquid plume develops mostly in a fluid which is still close to rest hence displays slightly less extension compared to B.
At the beginning of the expansion phase, see the middle picture in Fig.6, the TFE vortex seems to act as a barrier preventing droplets in configuration A to move forward throughout the expansion volume to get closer to the exit channel. At the same time, the liquid spray in configuration B has been split by the TFE vortex; most of the droplets follow the pressure gradient and are thus guided in the direction of the exit channel. At this stage the hot flow is interacting with the liquid in both configurations, the droplets diameter starts to decrease, as the evaporation process is enhanced.
Once the TFE vortex decays inside the expansion volume (see bottom picture in Fig.6), the mixing process between hot and cold fluid is completed. The liquid in the expansion volume for configuration A is kept on the back-side where the temperature is lower with respect to the center part. At the same time, for configuration B, the spray development is only mildly perturbed by the gas flow and the liquid plume extent is limited by the hot-core region. The oil vapour mass fraction is displayed in Fig. 7 at a time $t = 3.9\,ms$ corresponding to the expansion stage of the
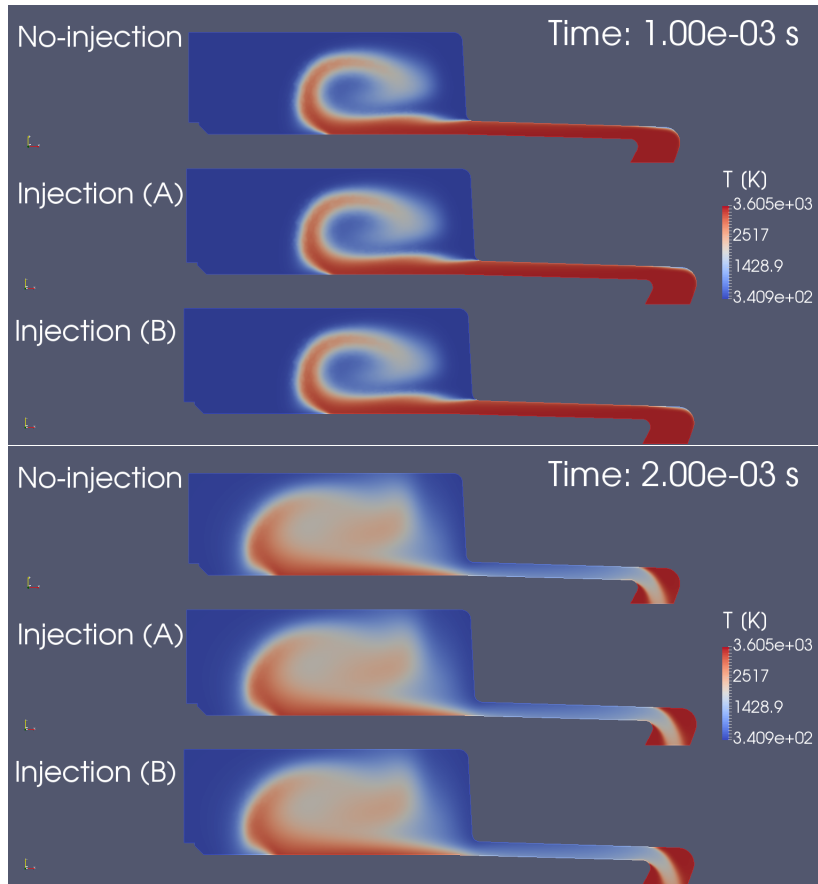
Figure 5. Temperature contours for the three configurations under study. Top : at $t = 1\,ms$; bottom : at $t = 2\,ms$.

flow. For configuration A, the vapour is still mostly present in the neighbourhood of the injection location because, as seen in the middle picture of Fig.6, the evaporating droplets are still mostly present in this region - the spray development being tempered by the TFE vortex developing in the chamber. For configuration B, a larger diffusion of oil vapour can be observed with oil vapour present in the channel and flowing towards the arcing region.

This qualitative analysis of the flow evolution inside the expansion volume can be completed with a more quantitative assessment of the spray performance with respect to the objective of delivering the chemical species brought by the spray to the arcing region. It is proposed to define the spray injection efficiency as the ratio between the mass of oil vapour delivered to a given section σ (typically the section connecting the channel to the expansion volume) and the injected liquid mass. Since oil vapour is created by the droplet evaporation process, this efficiency can be expressed as the following product :

$$\eta = \eta_{eva}\eta_{\sigma} \tag{1}$$

where η_{eva} measures the ratio between the oil vapour mass created by the droplet evaporation process and the mass of injected liquid oil

$$\eta_{eva} = \frac{m_{eva}}{\dot{m}_l(t_f - t_0)} = \frac{\int_{t_0}^{t_f} \left(\int_V \frac{\partial y_{oil}\rho}{\partial t} dV \right) dt}{\dot{m}_l(t_f - t_0)} = \frac{1}{\dot{m}_l(t_f - t_0)} \int_{t_0}^{t_f} \dot{m}_{eva}\, dt \tag{2}$$

and η_{σ} measures the ratio between the oil vapour flowing through section σ with respect to the total mass of oil vapour created in the expansion volume

$$\eta_{\sigma} = \frac{m_{\sigma}}{m_{eva}} = \frac{\int_{t_0}^{t_f} \left(\int_{\sigma} y_{oil}\rho\vec{u} \cdot \vec{n} d\sigma \right) dt}{\int_{t_0}^{t_f} \left(\int_V \frac{\partial y_{oil}\rho}{\partial t} dV \right) dt} = \frac{1}{m_{eva}} \int_{t_0}^{t_f} \dot{m}_{\sigma}\, dt \tag{3}$$

Figure 8 displays the evolution with time of $\dfrac{\dot{m}_{eva}}{\dot{m}_l(t_f - t_0)}$ for configurations A and B. Both configurations share an increase of the evaporation-rate up to a peak followed by a stabilization stage to a lower value but they also display

Liquid spray injection in the expansion volume of a CO_2 high voltage circuit breaker
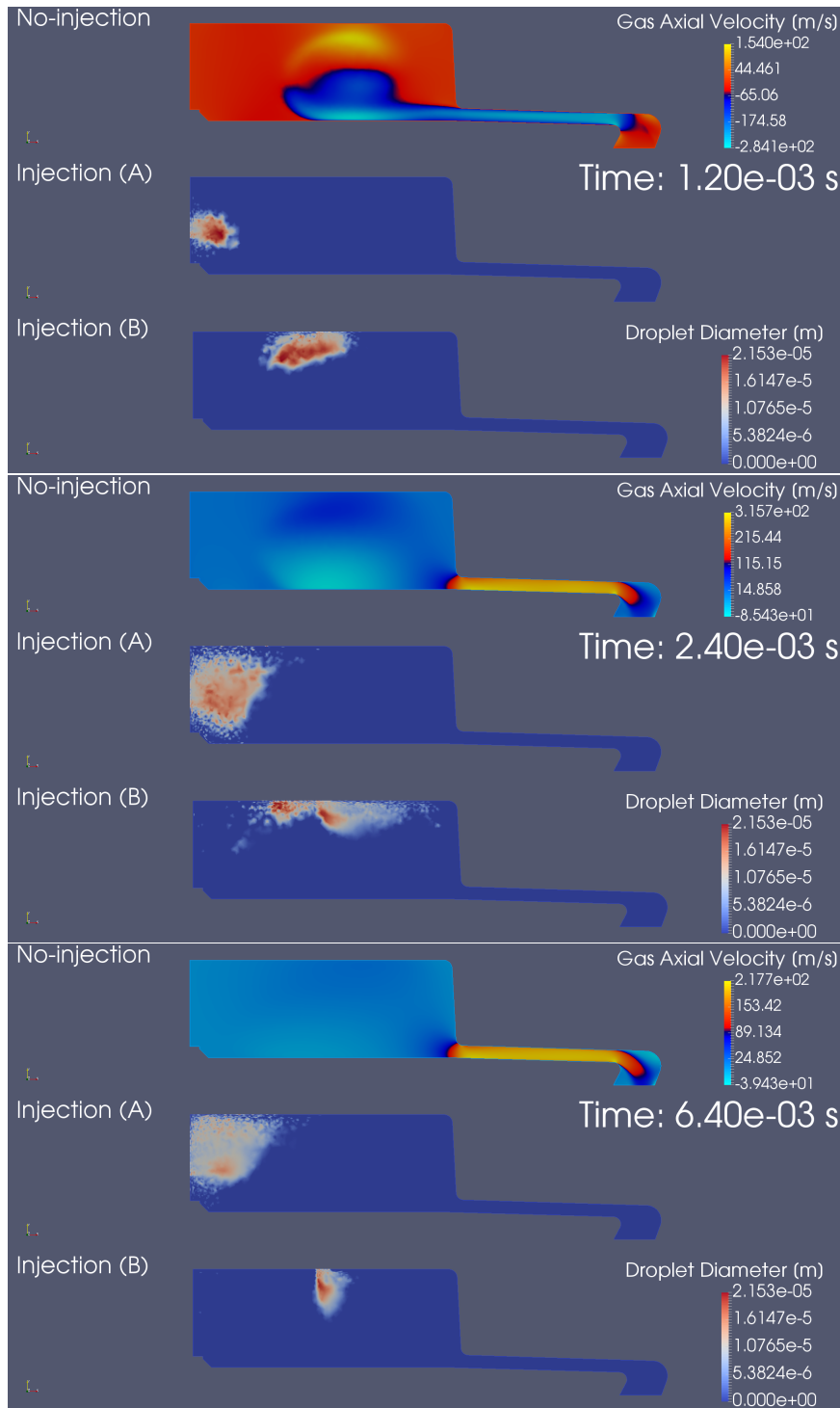
Figure 6. Carrier-phase axial-velocity for the no-injection configuration and contours of the droplets diameter for spray injection configurations A and B. From top to bottom : in-flow phase (top picture) followed by expansion phase (middle and bottom pictures).

a different dynamics. It can be indeed observed that evaporation starts slightly earlier in configuration B. For this configuration the hot gas reaches the liquid in advance with respect to configuration A, thus causing the peak of vapour generation around $t = 2\,ms$. As the hot-gas advances through the back-side of the expansion volume, the evaporation process takes place in configuration A as well. As previously observed in Fig.6, droplets in configuration A tend to accumulate in a colder region, thus their evaporation-rate increases slightly slower with respect to configuration B and reaches a peak at around $t = 7\,ms$. As the TFE vortex decays, the temperature becomes more homogeneous inside the volume, so that for both configurations a similar evaporation regime is eventually established after $t = 12\,ms$. Integrating these curves yields $\eta_{eva_A} = 0.80$ and $\eta_{eva_B} = 0.90$.
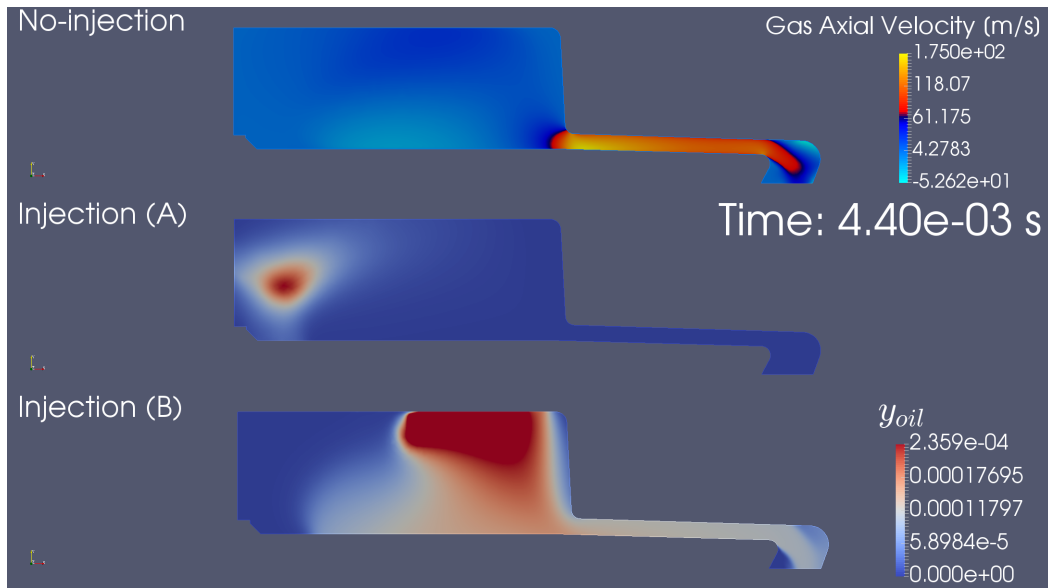
Figure 7. Carrier-phase axial-velocity for the no-injection configuration (top) and contours of vapour oil mass fraction for injection configurations A and B at time $t = 3.9\,ms$.
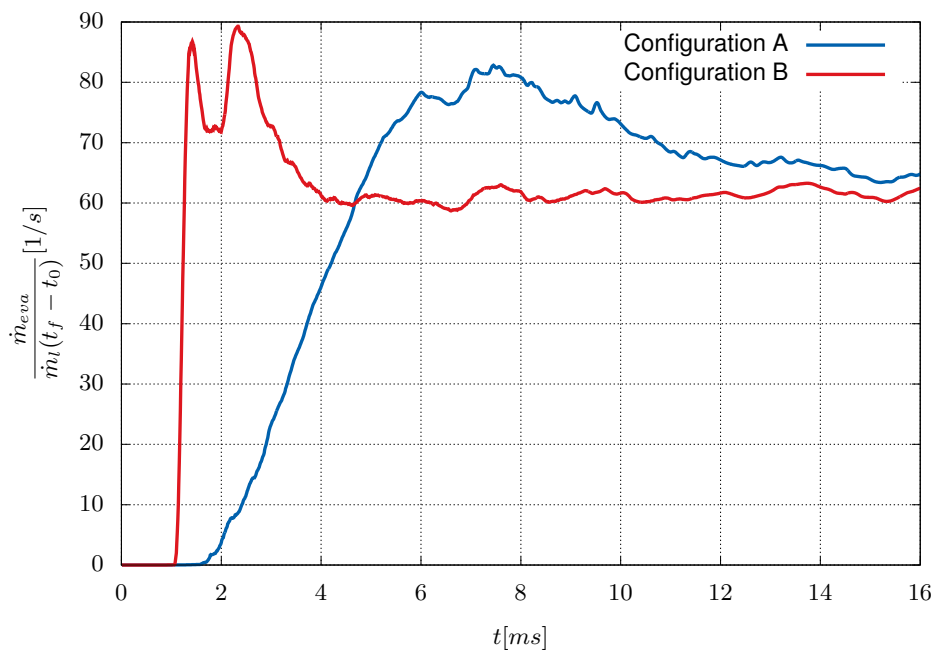

Figure 8. Evolution of normalized oil vapour production over time (until $t_f = 16\,ms$) for configurations A and B.

Furthermore in Figure 9 the variation with time of $\dfrac{\dot{m}_\sigma}{m_{eva}}$ is displayed for both configurations A and B. It is observed a greater amount of vapour oil flows towards the arcing zone in configuration B. Integrating these curves yields $\eta_{\sigma_A} = 0.005$ and $\eta_{\sigma_B} = 0.225$. Since it was deduced from Fig.8 the difference between η_{eva_A} and η_{eva_B} was rather modest, it can be concluded the B spray injection configuration is much more efficient than the A spray injection configuration - the detailed calculation yields $\eta_B \approx 50\eta_A$.

Conclusions

Eulerian-Lagrangian simulations of the interaction between an evaporating spray of mineral oil and the hot gas mixture (CO_2-C_2F_4) developing inside the expansion volume of a HVCB have been performed and analyzed. A transient pressure profile, obtained from a companion calculation of the whole HVCB system (including the arcing region), has been imposed at the boundary of the expansion volume in order to reproduce in a simple way the compression and expansion of the hot gas mixture inside the volume. It is thus possible to focus on the parametric analysis of the spray injection performance. In the present preliminary study, the influence of the spray injection
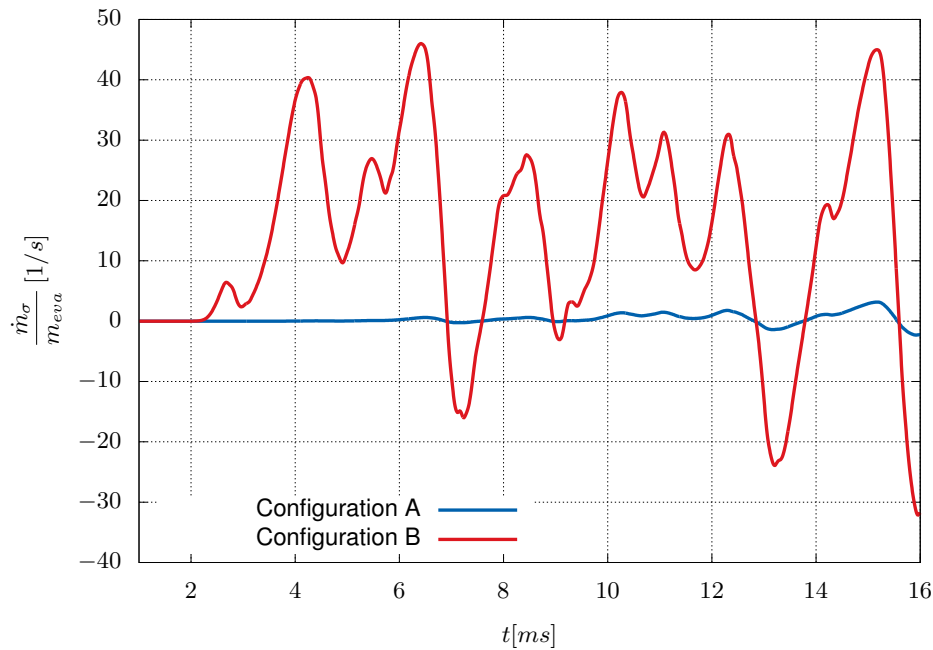
Figure 9. Normalized oil vapour mass-flow rate at $x/L = 0.7$ vs time. Blue and red lines correspond respectively to configurations A and B.

position has been assessed for two configurations A and B, corresponding respectively to a spray injection from the wall facing the inlet/outlet channel and from the top or outer radius of the expansion volume. Numerical simulations predict (and provide the physical understanding of this prediction) that both configurations produce a similar amount of oil vapour but the oil vapour is much less efficiently delivered to the arcing region for configuration A, resulting in an overall better performance expected from configuration B. Further studies will include injected spray characteristics derived from ongoing experiments.

References

[1] Riccardo Bini, Nils T Basse, and Martin Seeger. Arc-induced turbulent mixing in an SF_6 circuit breaker model. *Journal of Physics D: Applied Physics*, 44(2):025203, 2011.
[2] M. T. Dhotre, X. Ye, S. Kotilainen, M. Schwinne, and R. Bini. CFD simulation for a self-blast high voltage circuit breaker: Mixing and heat transfer. *2011 Electrical Insulation Conference (EIC).*, (June):528–531, 2011.
[3] Jong Chul Lee and Youn J. Kim. Effects of nozzle shape on the interruption performance of thermal puffer-type gas circuit breakers. *Vacuum*, 80(6):599–603, 2006.
[4] Markus de Hesselle and Jean-Yves Trépanier. Comparison of CFD Tools for SF 6 Self-Blast Circuit. *IEEE Transactions on Power Delivery*, 18(2):468–474, 2003.
[5] Youn-Jea Kim and Jong-Chul Lee. SF6 arc plasma simulation and breakdown performance prediction using computational fluid dynamics and arc modeling. *Thin Solid Films*, 521:206–211, 2012.
[6] Gary A. Dilts. Consistent thermodynamic derivative estimates for tabular equations of state. *Physical Review E - Statistical, Nonlinear, and Soft Matter Physics*, 73(6):1–15, 2006.
[7] M. Pini, A. Spinelli, G. Persico, and S. Rebay. Consistent look-up table interpolation method for real-gas flow simulations. *Computers and Fluids*, 107:178–188, 2015.
[8] F. Douglas Swesty. Thermodynamically consistent interpolation for equation of state tables. *Journal of Computational Physics*, 127(1):118–127, 1996.
[9] James Dakshina Gounder, Agisilaos Kourmatzis, and Assaad Rachid Masri. Turbulent piloted dilute spray flames: Flow fields and droplet dynamics. *Combustion and Flame*, 159(11):3372–3397, 2012.
[10] D. I. Kolaitis and M. A. Founti. A comparative study of numerical models for Eulerian-Lagrangian simulations of turbulent evaporating sprays. *International Journal of Heat and Fluid Flow*, 27(3):424–435, 2006.
[11] Hossam A. El-Asrag and Markus Braun. Effect of turbulence non-isotropy modeling on spray dynamics for an evaporating Acetone spray jet. *International Journal of Multiphase Flow*, 68:100–120, 2015.